Journal of Global Positioning Systems (2009)
Vol.8, No 1: 87-99

Journal of Global Positioning Systems
2009

Details of an Imaging System Based on Reflected GPS Signals and Utilizing SAR Techniques

M Usman, D W Armitage

School of Electrical and Electronic Engineering, The University of Manchester, UK

Abstract.

This research endeavor reveals a method for utilizing reflected Global Positioning System (GPS) signals to form an image of targets within a region of interest. The principle is based upon a type of bistatic synthetic aperture radar (SAR) in which a matched filter technique is employed to perform the image reconstruction. A major challenge was the appalling signal to noise ratio associated with the received reflected GPS signals. Moreover, the reconstruction method resulted in an undesirable point spread function (PSF) which degraded the reconstructed image. The entire GPS signal generation and image reconstruction process was simulated as faithfully as possible and it has been demonstrated that a spatial resolution of the order of the GPS L1 frequency (wavelength of 19 cm) is possible. The smeared image obtained due to poor quality PSF was improved by means of a Wiener filter based deconvolution method. An imaging system based on a stationary receiver has been practically demonstrated with the successful identification of a 0.5 m^2 spherical target.

Keywords: GPS, Imaging system, Bistatic synthetic aperture radar, Correlation.

1 INTRODUCTION

GPS was developed as a military navigation system with potential commercial applications (Kaplan). Direct GPS signals are utilized for the measurement of position and other navigation parameters with the help of dedicated hardware. However, reflected GPS signals, which are considered a nuisance factor in navigation, have the potential to be used for various remote-sensing applications.

The possibility of using GPS signals reflected from the Earth's surface as a new remote-sensing opportunity was first described in 1993 by the European Space Agency (Martin-Neira 1993) Similarly (Glennon) and (Cherniakov 2002) explored the idea of using the GPS as a bistatic radar illuminator for the purposes of air target detection. The reflected GPS signals can be used over the ocean to calculate mean sea height, wind speed, wind direction and significant wave height (James L Garrison 2002). Over land to measure soil moisture content, biomass and bistatic imaging (D Masters 2003) and over ice to ascertain ice age, thickness and surface ice density (A Komjathy 2000).

One of the pioneers in the effort of utilizing reflected GPS signals is J. Garrison of Purdue University, USA. His research primarily involved in finding and developing new applications of the Global Positioning System (GPS) and using the GPS signal itself as a remote sensing instrument (Stephen J. Katzberg and James L. Garrison).

The idea of 3D multi-static SAR imaging system, which utilized reflected GPS signals from objects on the Earth's surface was presented by Chris Rizos et al. (Yonghong Li 2002). The output of the matching filter was mentioned as:

$$S_{ij}(\tau) = \int_{-\frac{Ts}{2}}^{\frac{Ts}{2}-\tau} S_{Rij}(t+\tau)\, S_{Rij}{}^{*}(t)\, dt \qquad (1)$$

where T_s is the observation time, τ being the delay and $SR_{ij}(t)$ is the received signal and considered as an approximately linear FM signal. In fact, bistatic radar systems have been studied and built since the earliest days of radar. As an example, the Germans used the British Chain Home radars as illuminators for their Klein Heidelberg bistatic system during world war II. Fortunately, the advent of GPS solved many of the synchronization and timing problems that have

previously limited the performance of bistatic radar systems (Griffiths 2004).

M Cherniakov and co-authors have reported much work in the field of bistatic radars in general and utilizing different systems as transmitters of opportunity in particular. In an initial account they studied a Bistatic system with the aim to analyze the possibility of air target detection using bistatic radar and specified the associated problems and challenges (Cherniakov 2002). The research utilized the parameters of Iridium LEO satellite system and concentrated on the detection of air targets against a background of white noise, clutter and direct satellite signal. M Cherniakov et al. also examined the power budget analysis of signal detection in bistatic synthetic aperture radar, with global navigation satellite systems (GNSS) acting as non-cooperative transmitters (NCT) (Cherniakov 2002).

One of the key parameters around which a remote sensing system is designed is the spatial resolution. In the SAR system analysis of the point spread function (PSF) is used to characterize spatial resolution (Soumekh 1999). G P Cardillo used vector gradients to derive equations for range resolution, Doppler resolution and cross range resolution in meters and implemented them in computer code. The computer simulations for 1000 km altitude transmitter, with radar bandwidth of 500 MHz and integration time of 10 seconds showed the ground region for which the range and cross range resolution are each less than one meter (Cardillo 1990).

However, M Cherniakov et al. argued that these equations can only apply to the rectangular spectrum shape of the ranging signal (Cherniakov 2005). They based the resolution analysis with an introduction of BSAR spatial (Generalized Ambiguity Function) GAFs and first represented it in the delay-Doppler domain, and later on expanded to the spatial (coordinates) domain. Using this spatial presentation of GAF the range and azimuth resolution, as well as a resolution cell area are considered relevant to different directions and coordinate systems. Taking the idea further they presented equations of resolution of BSAR (Cherniakov 2003). With the assumptions that the target area and synthetic apertures are small, the transmitted signal is narrow band signal and used the stop-and-go approximation (Soumekh 1999). The equation derived for range resolution is: -

$$\delta_{range} = \frac{c}{2b\cos(\beta/2)} \qquad (2)$$

Where b is the bandwidth and β is the bistatic angle. The equation reveals that the highest resolution will he achieved for a monostatic case when β = 0 and range resolution is limited by the bandwidth of the transmitted signal. The theoretical range and cross-range resolution for the SS-BSAR has been mentioned as 5 meters and 10 meters respectively.

The authors are pleased to demonstrate that a spatial resolution of the order of GPS L1 wavelength (19 cm) is possible provided that sufficient coherent correlator integration time is allowed (in case of static receiver for at least two hours) and that the direct signals can be sufficiently suppressed for extended imaging range. However, the generated image exhibited significant blurring, this smeared image obtained due to poor quality PSF was improved by means of a Wiener filter based deconvolution method. In this context the deconvolution method is rather simplistic and this issue can form the basis of further research.

The author's research endeavor describes a bistatic SAR imaging system, which utilizes reflected GPS signals from targets and objects on the Earth's surface to form an image of the area of interest. The GPS satellites, a modified GPS receiver and its signal detection components, form the bistatic SAR system. Since the GPS satellites and / or receiver platform are in motion during the integration time, the signal obtained at the receiver position will be a Frequency Modulated (FM) GPS signal also termed as a chirp signal owing to the constantly changing Doppler shift.

The auto-correlation function of a chirp signal exhibits a narrow pulse property. We know from the basic radar concept that range resolution is an inverse ratio of the bandwidth of the signal. Chirp signals are the preferred transmitted signals used to obtain wide frequency band within a relatively wide time width. The linear FM pulse is called chirp signal and can be represented by the following simplified equation for a linear increase of frequency with time: -

$$f(t) = \cos(\omega_o t + \pi F/T\, t^2) \quad \text{for} \quad -T/2 < t < T/2 \qquad (3)$$

where $F = f_2 - f_1$ is the sweep bandwidth with f_1 and f_2 being the initial and final instantaneous frequencies and T is the time duration (Peyton Z. Peebles). It is possible for the bistatic SAR imaging system to obtain enough range and resolution simultaneously, since the frequency modulated GPS signal has superior pulse compression properties. A matched filter is employed in the received signal processing to improve system resolution. The matched filter is an optimum filter for signal detection in a white noise environment (Sklar 2001). Each reflected GPS signal is expected to have a unique chirp or signature which can be detected and coherently correlated with the direct signal provided that the geometry of the satellite is optimum. The location of the target will have a strong correlation value and can thus be identified in the area of interest. Detailed simulations and later on practical experiments have revealed that the bistatic SAR system has the potential to develop acceptable quality and low cost images of a localised area.

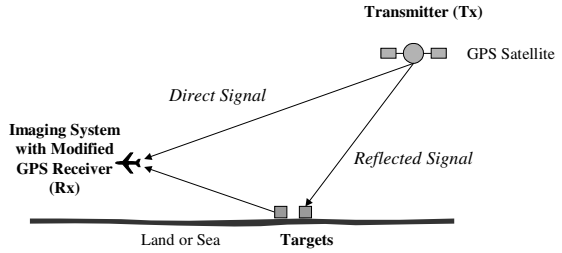

Figure 1: Imaging scenario - Airborne receiver

The concept of generating an image by the correlation of direct and reflected GPS signals is based on the SAR principle in which the receiver or bistatic radar is required to sustain its movement in spatial domain. There can be three different types of imaging scenarios based on the source of synthetic aperture, receiver kept airborne, ground moving receiver and static receiver.

The transmitter, target and receiver geometry in case of an airborne receiver can be understood with the help of figure (1), as per the traditional SAR concept the receiver is kept airborne and can detect the presence of ships or other terrestrial targets. The second option is to mount the imaging system on a ground vehicle and drive along a target thus simplifying the geometry and eliminating the need for airborne platform. However, the requirement for precise receiver position and velocity and associated logistics issue rendered this option non-practical.

In order to simplify the experimental set up, it is possible to generate an image with a static receiver, at least theoretically, if sampling is performed over longer period of time, such a scenario is depicted in figure (2). With the receiver being static the change is geometry is provided by the moving GPS satellite, though the change in geometry is a relatively slow process and results in very long data acquisition times of the order of hours. One of the numerous possible applications with this type of set up are remote sensing for monitoring of landslides, long-term seismic studies and similar applications.

The possibility of using this technique for imaging purposes has been mentioned in various research papers as a number of institutions study bistatic SAR with asymmetric configuration, but there is little information regarding detailed simulations to confirm technical feasibility or experimental results. In this context the efforts carried out to simulate and practically validate the results with the help of static or stationary GPS receiver are a novel achievement. Nonetheless, simulation details and relevant problems, shortcomings and challenges have been recorded for all three scenarios that can prove beneficial for later research efforts.

The main objective of the author's research was to model these imaging arrangements and scenarios in a software environment with the aim to remove major existing bottlenecks, optimize the design and later on, attempt to assemble a proof of concept hardware of the imaging device in order to demonstrate a practical system.

The purpose of this research paper is to elaborate how this goal was achieved by careful antenna design, suitable electronic circuit, appropriate GPS signal acquisition and tracking algorithms and efficient reconstruction code. The document explains the efforts put forward to generate an image by the correlation of direct and reflected GPS signals and based on bistatic SAR techniques.

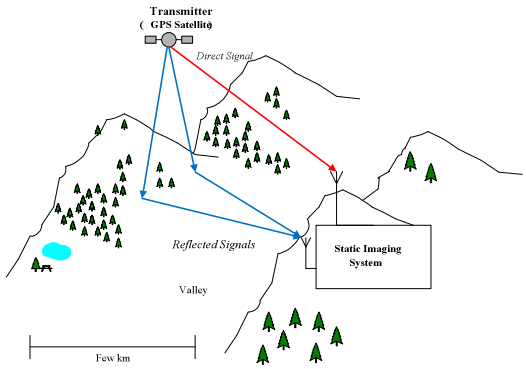

Figure 2: Imaging Scenario – Stationary receiver

There are many advantages of this type of system (a) GPS target detection and imaging has the attraction that the user can take advantage of the expensive GPS infrastructure maintained for navigation purposes by employing it as a 'illuminator of opportunity' thus there is no requirement for a dedicated transmitter. (b) There are several measurement opportunities, one for each GPS satellite in view, thus forming a multi-static radar system. (c) The imaging system has the additional advantage of being very cost effective, as it can be built for a fraction of the cost of traditional radars, space-borne equipment and other sensors. (d) The operation will be covert as no signal will be transmitted locally unlike mono-static radar. (e) Bistatic radar may also have a counter stealth capability, since target shaping to reduce the mono-static RCS of a target will in general not reduce its bistatic RCS (Griffiths 2004).

We know that power spectral density of any given GPS C/A code signal is below the power spectral density of noise. It is converted to a usable (signal to noise ratio) SNR by correlation of a locally generated C/A code sequence that provides an effective processing gain to the SNR ratio. The theoretical processing gain for the C/A code is 1023 or 30.1 dB (Kaplan). High autocorrelation peak and low cross-correlation values provide a wide dynamic range for signal acquisition. Hence, on the basis of correlation theory the code is able to be detected, although it is buried in noise. This important property of the GPS signal plays a vital part in our simulation to detect the target with the help of reflected GPS signals (M. Usman 2006).

When the GPS signal arrives at a target, it is reflected in a manner that depends on the surface roughness and the dielectric properties of the target. The reflected signals that are of most use for imaging purposes are those reflected in a non-specular manner. Such a 'reflection' results from the signal being scattered over a wide angle, and will thus be subjected to further attenuation as a function of distance traveled. We could consider the surface of a complex target to consist of a number of 'point reflectors'. In reality 'point reflectors' must have finite size, and for our purposes it would seem expedient to model these 'point reflectors' as spheres with a diameter comparable to the resolution of the imaging method.

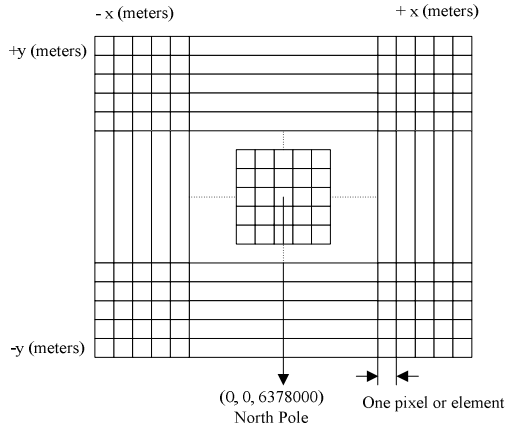

Figure 3: Candidate position for the target

2. SIMULATION

The simulation work was carried out in a Matlab® environment and during initial phase of the research a simple code was generated in order to verify the imaging principle and concept. After successful initial simulations, the code was modified and expanded to facilitate image generation under practical scenario and efforts were put in to improve the computational efficiency.

The simulation was deliberately split into two distinct parts: the first part being responsible for synthesizing the signal emanating from the analogue to digital converter of the GPS front end, the second part being responsible for the image reconstruction. Care was taken to ensure that the only information available to the reconstruction engine was the digitized GPS signal, and 'globally available' data such as the satellite ephemerides and the receiver location. The signal synthesizer determines the satellite orbits together with the individual PRN code offsets and combines the direct signals from all satellites in view with the reflected signals from the targets together with the receiver noise. Transit delays associated with the signal paths are calculated based on satellite and receiver trajectories.

The reconstruction engine divides the region of interest into an array of square bins and attempts to coherently correlate the received signal with an individual template chirp unique to each bin. Only where the received signal contains a matching chirp does a given bin achieve a high score. In order to generate the matching templates, the reconstruction engine independently calculates the signal transit delays and PRN codes in the same way as the signal synthesizer, but for all candidate target locations.

The search area in which the targets can be located is shown in figure (3). The position (0, 0, 6378000) in ECEF coordinate system was fixed in the middle of the search area. These are actually the coordinates of North Pole, employed to simplify coordinate transformations.

The matched filter processing plays a vital part in the simulation. In the Matlab environment this is performed by multiplying two signals sample by sample and than accumulating. The process was carried out for each sample and the relevant value was stored in the form of a two dimensional matrix. The matrix was scanned for each sample in time, rendering the procedure equivalent to a matched filter process. A different value of correlation was obtained for each instant in time. The location of a target is expected to have a maximum value of coherent correlation. A grey scale image was constructed using above-mentioned information. Thus, the image produced directly pin points the target at the desired coordinate in the candidate position.

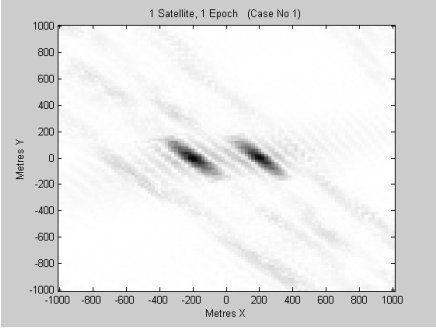

Figure 4: Results for integration time of 0.1 sec.

3. RESULTS AND ANALYSIS

The Matlab® simulations were carried out under different conditions and scenarios by varying various parameters. Initially an integration time of 0.1 seconds was selected and the results were comparable to that presented in (Yonghong Li 2002).

As depicted in the figure (4), the two targets can easily be recognized with acceptable spatial resolution. For the next case the integration time was increased to 0.2

seconds, although the simulation took many hours longer to execute but resulted in improved resolution. The longer integration time produced larger number of samples and improved the PSNR (peak signal to noise ratio) in the reconstructed image.

As mentioned earlier the other configuration for this type of system would involve a static GPS receiver. Figure (5) reveals that the resolution was limited only by the image pixel size of 20 m in case of such a scenario, when sampling is performed every few seconds over a longer period of time, for example six hours and later on integrated. The targets are clearly visible with no distortion. In fact the longer integration time has resulted in larger number of samples and cancellation of uncorrelated noise.

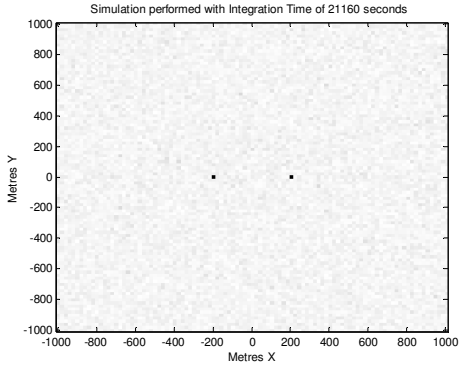

Figure 5: Results for integration time of 21160 sec (6 hours)

3.1. Direct Signal Suppression

Under practical scenario the strength of GPS signal is very low and buried in noise and only with the help of correlation theory and deterministic nature of the GPS C/A codes the signal is detected. The reflected signal is even weaker but it is expected that the targets can be resolved by integration over longer periods of time. However, in case the reflected signal is further reduced, due to the type of reflecting surface and distance covered, it can become equal or lower than the tails of auto correlation function of direct signal and can be permanently lost. No matter how long we integrate the reflected signal cannot be separated and the targets are no longer resolved. This phenomenon can be understood with the help of the figure (6).

In numeric terms, the tails of autocorrelation of direct signals are 24dB lower than the direct signal peak. Theoretically, the reflected signal must not be lower than 24dB as compared to the correlation peak of direct signals.

Simulations were performed to explore the limits within which the targets can be resolved in terms of the magnitude of the direct and reflected signals. The direct signal was attenuated to a significant amount in an effort to find out the threshold of target detection, the indirect signal was also attenuated in incremental form. It was deduced that in order to bring both signals comparable in terms of magnitude and make sure that the autocorrelation tails of direct signal are smaller that the reflected signal it is imperative to attenuate and scale down the direct signal. It is assumed that this large suppression figure could be achieved by a combination of careful antenna design and signal subtraction within the signal processing, since the receiver channel for the reflected GPS signals may be locked to the direct signal. Other options including the utilizing of multi-beam antenna with main lobe for the reflected signal and side lobe for the direct signal can be explored.

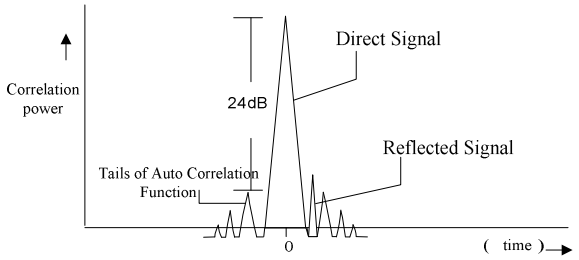

Figure 6: Correlation of direct and reflected GPS signal

However, there are some simple ways to improve the SNR of the reflected signal, for example, carry out correlation for longer period of time, use high gain directional antenna or perform image processing at a shorter range. These simple measures have been adopted in the initial practical experiment carried out to acquire data for image generation purposes. A high gain and directional antenna for acquisition of reflected GPS signals was employed and the range was kept short. This resulted in strong reflections from the spherical target covered with aluminum foil and the reflected signal was comparable in magnitude with the direct signal. However, in case of extended data acquisition ranges where weak reflected signals are received, this issue has to be kept in mind.

Other researchers working in the related field also came across this issue and have referred to it in terms of direct path interference (DPI) and cross correlations. M Cherniakov et al. explained that taking into account only one satellite as the source of DPI, traditional adaptive side lobe cancellation methods can be applied for DPI suppression (Cherniakov 2005). In a related study E P Glennon provided a brief description of the GPS cross correlation problem and sketched a comparison between the cross correlation problem as experienced by GPS and the CDMA cellular communications. He examined several different types of cross correlation mitigation techniques, ranging from successive interference cancellation through to subspace projection methods and showed that the mitigation techniques are also applicable

to the removal of autocorrelation side lobes (E. P. Glennon).

3.2. Accuracy of the ADC (Analogue to Digital Converter)

In order to perform necessary signal processing the GPS signal is to be converted to digital format after down conversion from RF of 1.575 GHz to a manageable IF of a few MHz. This process is to be performed by the Analogue to Digital Converter (ADC). The best possible bit accuracy for the ADC was calculated by Matlab® simulations. It is imperative to consider that a higher than required accurate device will lead to unnecessary expensive and complex hardware and a burden on the computation power in the simulation process. On the other hand an inferior ADC will result in signal degradation. It was deduced that at least two bits are required as the minimum accuracy. This was an important result and proved that a commercial off-the-shelf GPS receiver can be used as RF front end in the imaging hardware. The reason for results obtained was due to the fact that variance of quantisation noise (σ^2) = q^2 / 12, where q is the step size or (Least significant bit) LSB and hence Standard deviation (σ) = q / $\sqrt{12}$ = q / 3.5. For two bits there are four level (2^{N-1}) and for one bit only two levels are present, hence quantization noise will become double and comparable to the thermal noise in the signal.

3.3. Improvement in Computational Efficiency

It was observed that the Matlab® simulations were very expensive in terms of computation time and memory and will be feasible only for off-line applications. One of the many methods of improving the computational efficiency is by switching from interpretive Matlab® to compiled code. In order to improve the speed of the program a modular approach has been employed. The GPS signal was generated separately in C++ environment using the Borland C++ Builder. The program simulated all the functions of the Maxim MAX 2741 IC used as the RF front end in the hardware. This approach speeded up at least the signal generation part of the code by a factor of about 9. The reconstruction code developed in Matlab® was also modified in an effort to make it more suitable for a practical scenario. In order to improve the computational efficiency the calculations were performed on linear arrays (or vectors) rather that multi-dimensional arrays. The block diagram of the reconstruction algorithm is depicted in figure (7).

As evident from the diagram the two signals (locally generated and received GPS signals) are multiplied and added at each segment and a different value of correlation is obtained for each instant in time. The value is stored in the array by suitable Matlab® commands. However, the values of the delay and offset PRN for the locally generated or reference signal are to be calculated first.

These parameters are determined by measuring the distance between reference satellite to candidate position and receiver to candidate position. The delays are calculated not for a particular target position, but for all candidate positions in the area of interest. The simulation calculated the delay from satellite to the receiver for each box or segment as shown in the figure (8).

Initially, this represented a two-dimensional array representing delays for each candidate position. The code also calculated the delay offset from the centre and considered it as a reference, utilizing it for comparison of the offset values. First of all, the code calculated the delays at the midpoint of the segment as a reference and stored the value for each candidate position. The delay-offset range is also determined as an offset to delay at centre or midpoint of segment.

A template was generated in the form of a linear array or vector of delay offsets relative to the image centre with initial value as minimum value of delay offset and final value as the maximum of delay offset. The template for direct signal was represented as follows:

$$S_{dir} = d_{dir}(t)e^{jwL_t} \tag{4}$$

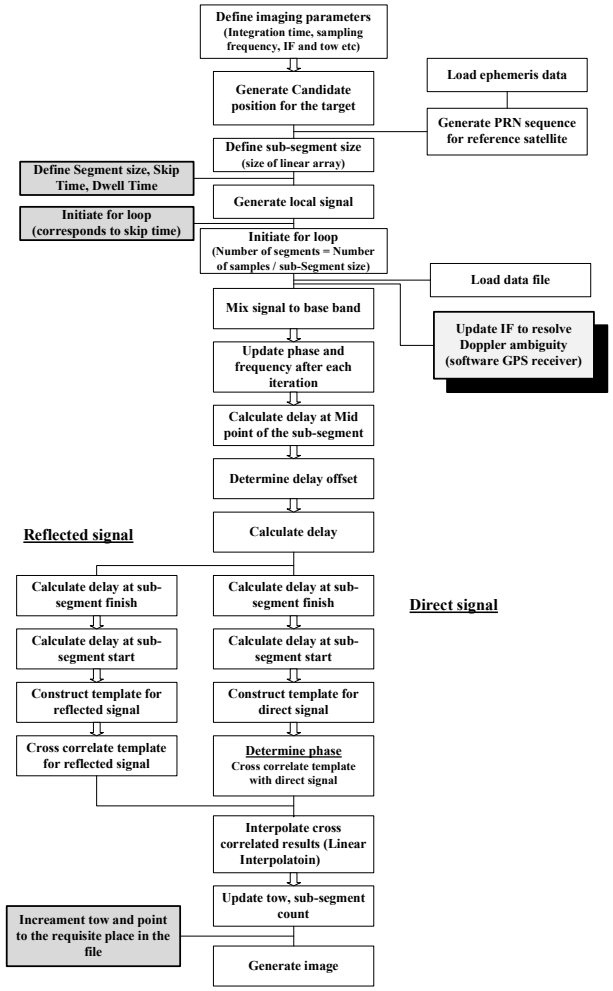

Figure 7: Block diagram of the reconstruction code

where $d_{dir}(t)$ is the C/A code for direct signal after offset has been introduced and w_L is GPS L1 frequency in radians / seconds. The template was cross-correlated with the direct received signal to determine the phase difference.

Similarly the template for reflected signal was represented as follows:

$$S_{ref} = d_{ref}(t)e^{jw_{L1}} \tag{5}$$

where $d_{ref}(t)$ is the C/A code for reflected signal after offset has been introduced.

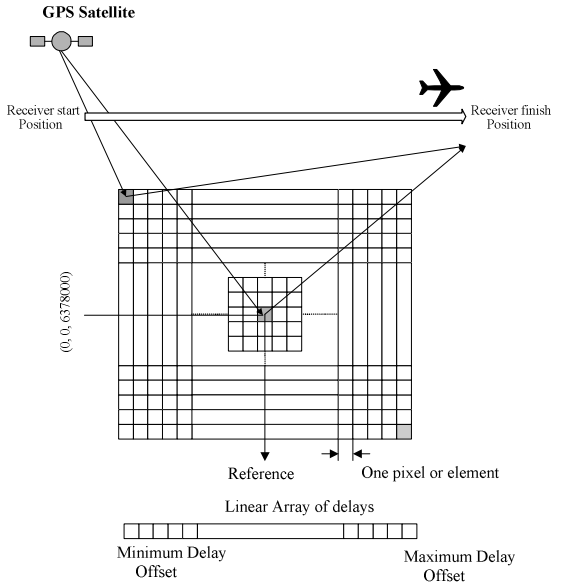

Figure 8: Calculation of Delays and Interpolation for Linear Array

The reflected signal was cross-correlated with the template for reflected signal and results were interpolated to form a linear array. The method used was linear interpolation, which can be represented by the following equation.

$$w(n+\eta) = (1-\eta)w(n) + (\eta)w(n+1) \tag{6}$$

where n is the integer part of the original index value and η is the fractional part (Smyth February 18, 2008).

Thus by calculating for each location, an array or vector was formed which contained all the linear representations of the range of possible wrapped signals. Owing to the one dimensional array, there are fewer calculations while the correlation is performed, but the simulation still took a long time as the new calculations are more complex. Never-the-less even with improved resolution as mentioned in the next section there was a further improvement of computational efficiency by a factor of 2 to 4.

Another method to improve the computational efficiency was signal segmentation, which was incorporated in the code to simulate low velocity and static or stationary GPS receiver. Only selected amount of data was processed, while the rest was omitted and the phase, frequency and TOW (time of week) were updated accordingly. However, the method can be used for any imaging arrangement and the fact that only part of the signal acquired is processed for image generation, the technique resulted in reduced computational time but comparable image quality.

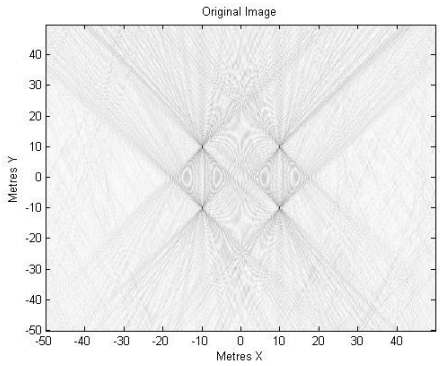

Figure 9: Raw reconstructed image

There is a simple method to improve computational efficiency, which is sub-sampling or under sampling. In the reconstruction algorithm a built in Matlab® function resample was used to perform sub-sampling (up to a factor of 10), thus reducing amount of data to process and in turn improve computational efficiency, without compromising image quality.

3.4 Resolution

In order to test the achievable resolution the simulation space was represented by an array of 400 x 400 bins with pixel dimensions of 25 x 25 centimeters. Four point reflector targets ware placed on the corners of a 20 m^2 area, having coordinates (10, 10, 6378000), (-10, 10, 6378000), (-10, -10, 6378000) and (10, -10, 6378000). Each conducting point reflector had an effective radius of 10 centimeters and reflection coefficient of 1. This particular value for the radius was selected to demonstrate that it is possible to detect a target comparable to the 20 cm wavelength of GPS L1 frequency. It was assumed that the antenna for reflected signals has a gain of 30 dB and that the direct signals can be suppressed by 70 dB. The coherent integration time was set to 10 seconds.

The generation of image with the modified reconstruction algorithms (receiver velocity of 200 m/s and sampling frequency of 2 MHz), as shown in figure (9), revealed two conspicuous conclusions, firstly the targets appeared to have the potential of being resolved to the size of one bin, and secondly there was significant blurring. It is pertinent to note that despite the targets exhibiting a star-like PSF, achieving a resolution comparable to the wavelength of GPS L1 frequency is a novel achievement. According to the author's knowledge it has not been documented anywhere in the research literature.

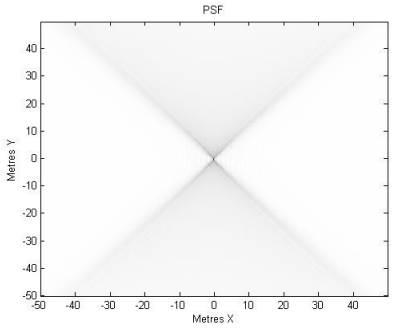

Figure 10: Point Spread Function

3.5. Image Restoration

The image-processing task at hand was to reconstruct the unfocused target signature into a focused image. A technique of de-convolution of the signal with its PSF using Wiener Filter has been employed to correct the blurred image obtained form two isolated point reflectors. In our simulation we know the signal and also calculate the PSF of the signal in order to utilize this filter. The point spread function is calculated during the course of simulation and used as the degradation function and is shown in figure (10).

During the simulation white noise is assumed, whose power spectrum is constant, which simplifies things considerably (R. C. Gonzalez 2002). The Wiener Filter in Matlab® is based on the following equation with value of K selected as 10^{16}.

$$\hat{F}(u,v) = G(u,v)\left[\frac{H^*(u,v)}{|H(u,v)|^2 + K}\right] \quad (7)$$

Where F(u,v) is the input image, G(u,v) is the degraded image and H(u,v) is the spatial representation of the degradation function in the frequency domain and H*(u,v) is the complex conjugate of H(u,v). The restored image in the spatial domain is given by the inverse Fourier transform of the frequency domain estimate. The deconvolved and reconstructed image is shown in figure (11). Further details in this regard have been documented in (M Usman 2008).

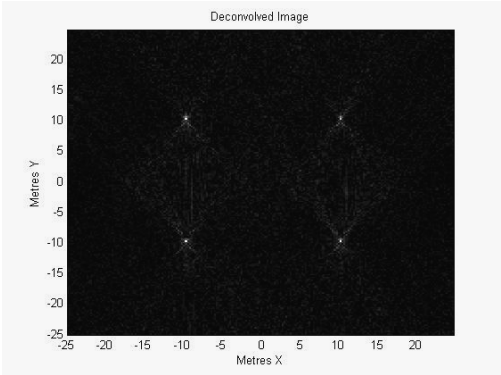

Figure 11: Deconvolved and reconstructed image

3.6. Simulations for Static GPS receiver

As mentioned earlier for static receiver configuration the change in geometry to generate the synthetic aperture is provided by the moving GPS satellites, which have an average orbit altitude of 20,200 km above the surface of Earth and complete one orbit in approximately 11 hours and 58 minutes (Kaplan). For the orbiting GPS satellite to provide the requisite synthetic aperture, GPS data in the order of hours is required. However, storage of such huge amount of data is not practical.

Fortunately, not all acquired data was utilized and it was necessary during image reconstruction to process selected amount of data while omitting other and updating the phase, frequency and TOW (time of week) accordingly. This resulted in dividing the GPS IF data into smaller parts or chunks denoted as skip time (T_{sk}) and dwell time (T_{dw}). The former represented the time interval during which data is not processed or omitted in order for the change in geometry to become effective or build up. The latter denoted the time during which the reconstruction algorithms process the GPS data for correlation of direct and reflected signals in order to generate an image.

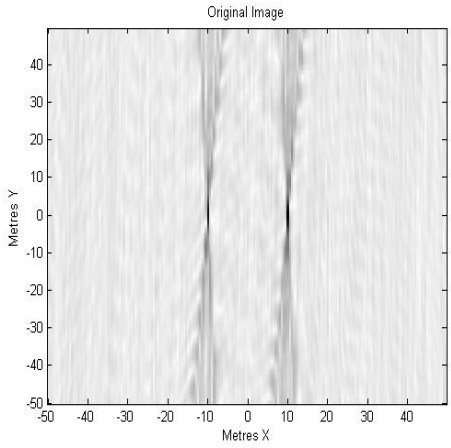

Figure 12: Simulation results for 7200 seconds

Detailed simulations have revealed that at least one hour (3600 seconds) of integration time is required to successfully resolve the targets with acceptable spatial resolution. However, two hours of data furnished a sub meter level range resolution, as depicted in figure (12). The image quality is directly proportional to the physical change in geometry of the GPS satellite, thus the resolution and quality of image depends upon the total integration time.

4. THE IMAGING HARDWARE

The imaging scenario is shown in figure (13). It is apprized that the reflected signal is not expected to have enough SNR to permit successful signal acquisition. So the direct signal from a specific satellite received by the RHCP antenna has been selected, locked and used as a reference for the reflected signal.

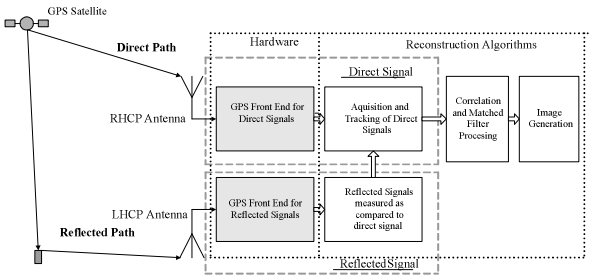

Figure 13: The Imaging Scenario

Once successful lock is achieved, the same local oscillator can be employed for the direct as well as the reflected signal. The GPS signals are received, amplified, down-converted and digitized into near base band samples, which are than processed using software routines to acquire and track the direct GPS signal and later on matched filter processing with indirect signals culminate the task of image generation.

In order to perform the field trails a custom LHCP helical antenna and two-channel GPS front end and data capturing device for acquisition of GPS signals has been prepared. The antenna furnished a compact size and high gain solution for signal acquisition. More importantly being of reverse in polarization as compared to direct signals and pointed away from GPS satellites, it delivered excellent immunity against direct signal interference.

The design requirement for the data collection device of the imaging system was a low-noise, dual-input receiver operating at the frequency (L1) used by the GPS satellite signal. Initial design reviews led to the adoption of two MAX2741 IC's as the basis of the design. The IC is an L1-band dual-conversion GPS receiver which down converts the 1575.42MHz L1-GPS signal to a 37.38MHz first (Intermediate Frequency) IF, and then a more manageable second IF of a few MHz. The on-chip Analogue to Digital Converter (ADC) samples the down-converted GPS signal at the 2nd IF with the rate of 19.2 MSPS. Sampled output is provided in either 2-bit (1-bit magnitude, 1-bit sign) or 3-bit (2-bit magnitude, 1-bit sign) formats, as determined by the ADC mode configuration bit.

As depicted in figure (14), one front end of the device receives the direct GPS signals, while the other receives the reflected signals through the LHCP antenna. Further

details regarding the imaging hardware have been documented in (M Usman 2008).

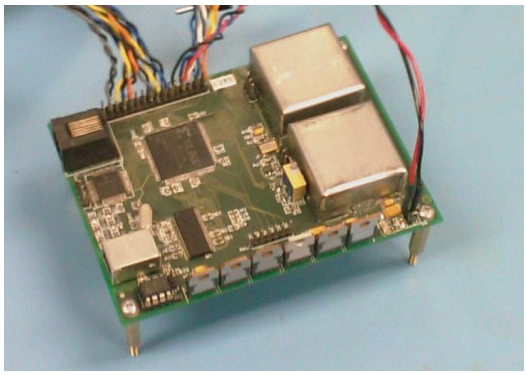

Figure 14: Two-channel GPS front end and data capturing device

5. GPS DATA ACQUISITION AND IMAGING

In order to test both channels of the GPS front end and data capturing device and to confirm that the signal received by the LHCP antenna is in fact the reflected signal an experiment was performed in front of a large brick building. The LHCP antenna was positioned so as to receive the signal bouncing off the building. A Wi-Sys inline amplifier of gain 30 dB was used to amplify the weak reflected GPS signals.

As expected a very strong signal was received with the RHCP GPS antenna, yielding good acquisition even for few ms of integration time. The comparatively weaker reflected signals acquired by the LHCP antenna required much longer integration times (200 ms) to achieve comparable SNR. Longer acquisition time results in the cancellation of uncorrelated noise, thus improving the SNR. The Doppler frequency of both signals is the same but code offset is slightly different corresponding to the extra distance that the reflected signals have to travel.

The length of one GPS C/A code is 1023 chips and is transmitted with a frequency of 1.023 MHz. Taking into account the speed of light the length of one chip can be calculated to be 300 m. As mentioned above the signal is sampled at 19.2 MHz. Thus each code sample corresponds to about 15 meters. It is possible to distinguish between the direct and reflected signal if the path length between direct and reflected signal is a multiple of 15 meters.

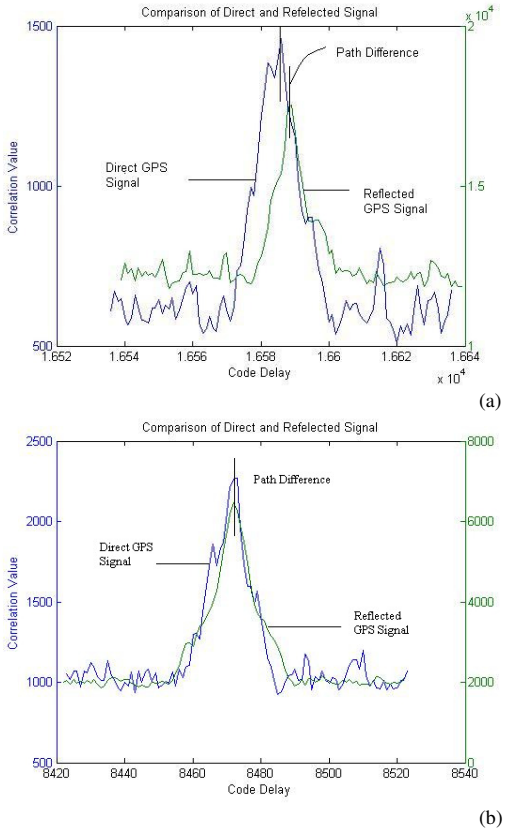

Figure 15: Comparison of direct and reflected GPS signals for (a) 50 m (b) 4 m (round trip distances)

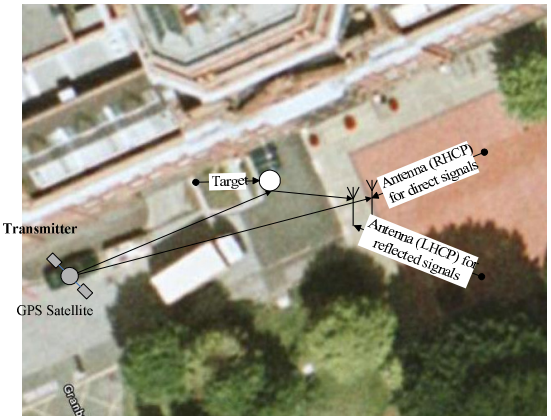

Figure 16: Location of both antennas and the target

During the experiment performed the difference in code samples of direct and reflected signal was 3 or 4 which came out to be about 45 to 60 meters and corresponds to the round trip distance between antenna and the large brick building or reflective surface. Figure (15a) compares the direct and reflected signal correlation peaks clearly depicting this path difference. The scale for the correlation value (y-axis) is different for both signals on account of the varying acquisition time.

In order to verify the results, GPS IF data was collected at a position of only two meters away from the building or reflecting surface. A path difference of only one code samples was observed among the direct and reflected signal as shown in figure (15b). A near specular GPS reflected signal was received suggesting an optimum geometry for reception of reflected signals. Thus the experimental results substantiated that the signal present at the LHCP antenna is in fact the reflected signal and construction of the hardware has been successful.

After successfully simulating the static receiver imaging scenario, modifying the reconstruction algorithms to process longer duration GPS signals and acquiring the reflected GPS signals. The imaging hardware including the two antennas and data acquisition device was positioned in front of the University building, the location of the direct and reflected antennas and target are shown in figure (16). A $0.5m^2$ spherical target wrapped in aluminum foil was placed in front of the university building.

During acquisition of data for imaging purposes the nearby buildings formed an urban canyon type environment thus limiting a clear of the view of the sky. The most suitable satellite (in terms of signal strength and visibility) was GPS BIIRM-2 (PRN 31) and was therefore selected as the reference satellite.

A comparison has been made between the acquisition diagram for 5 ms of direct signal and 100 ms of reflected signal in figure (17). The coarse frequency of both signals is the same but code offset is slightly different corresponding to the extra distance that the reflected signals have to travel. During analysis of individual data files, this difference fluctuated between one or two code samples (may be due to the quantization effect of the ADC) corresponding to a path difference of about 20 meters between direct and reflected GPS signals.

In order for the GPS satellite to provide the requisite change is geometry, 80 files were down loaded at an interval of about 30 seconds each. The length of individual file was 4 seconds, but only the first few milliseconds of each file were used during the reconstruction process. During simulations it was deduced that a 30 seconds interval among the acquired files is just enough to resolve the targets.

The GPS data provided about 2400 seconds for change in geometry, just enough to identify the target, but compromising the resolution. Figure (18) compares the image by reconstructing 2400 seconds of actual data with a simulated signal of 2400 seconds. In future it is recommended to perform signal acquisition in an open environment to have a clear view of the sky and thus increasing the chances of receiving more GPS satellites and for extended duration. The target can be seen in the middle of the diagram, as the antenna's main lobe was aimed roughly towards the target center. Unfortunately, an increase in the integration time also resulted in more signal being received by the highly directional antenna and some of the signal was not received from the target, but bounced off from nearby objects and building front.

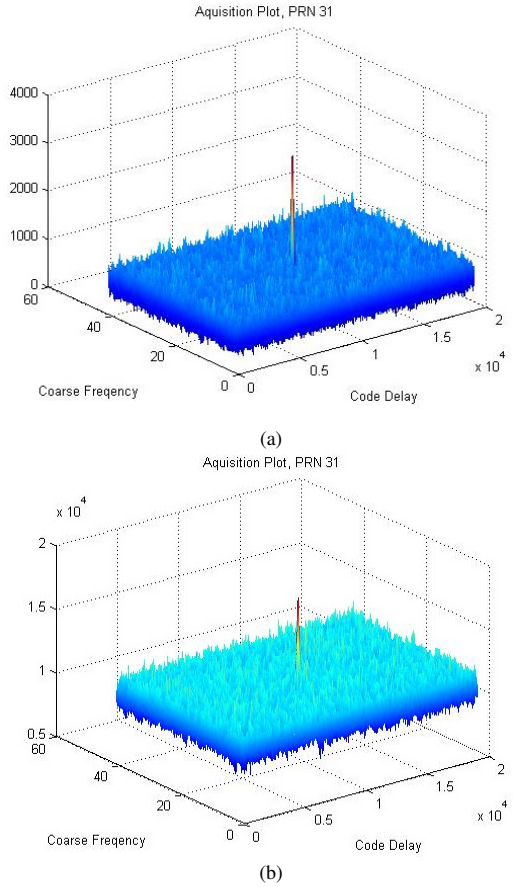

(a)

(b)

Figure 17: Comparison of acquisition plot (PRN 31) for acquisition time (a) of 5 ms for direct signal (RHCP antenna) (b) of 100 ms for reflected signal (LHCP antenna)

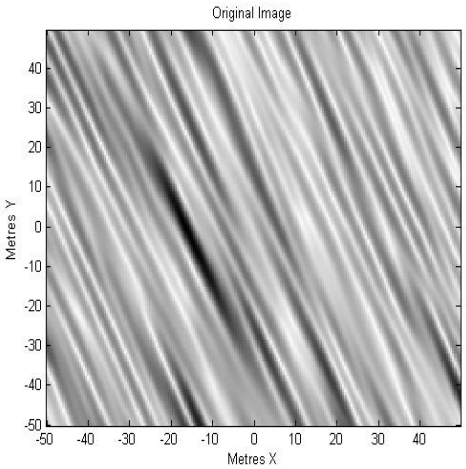

(a)

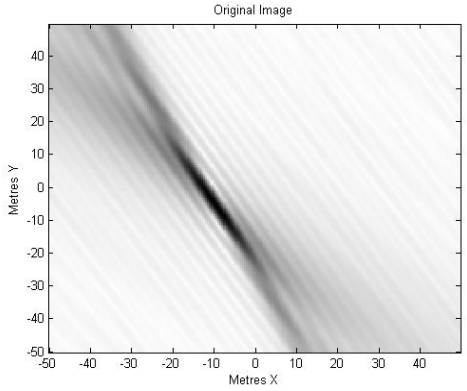

(b)

Figure 18: Comparison of image obtained by reconstructing 2400 sec of (a) Actual signal (b) Simulated signal

As evident front the results, although it is roughly possible to distinguish the target, there is excessive backscatter or clutter and noise exhibited in the images. The situation was exacerbated due to the fact that the high gain LHCP antenna was placed in front of a large brick building. The antenna was designed to acquire the weak reflected GPS signal, but returns from objects around the target were also received and displayed in the image. As mentioned earlier that due to hardware limitations, the data files were acquired after an interval of every 30 seconds each, such low frequency for acquiring temporal samples induced an aliasing effect. In future it is recommended to modify the imaging hardware to acquire GPS data after every three seconds.

The exhibited images may seem very primitive, but it has to be kept in mind that no dedicated radar transmitter was available during the experiments. The target has been detected in a hostile environment with the help of extremely weak reflected GPS signals that are omnipresent, but exhibit an appalling SNR. It is further apprized that the change in geometry to process the data with the help of SAR technique was provided by the orbiting GPS satellite. This particular method has so far not been utilized in a practical environment for imaging purposes.

Although steady progress was made during research endeavor and an image of the area of interest, roughly identifying a 0.5 m^2 sphere target was generated. Extensive field experimentation with the imaging device needs to be performed. In order to confirm the detection of target, more data is to be acquired at a suitable location that ensures visibility of the reference GPS satellite for at least two to three hours for a high resolution image. The resolution can be improved by correlating for longer periods of time and correcting the relative phases of direct and reflected GPS signals.

6. CONCLUSIONS AND RECOMMENDATIONS

During the course of current research endeavour, the entire GPS signal generation and image reconstruction process has been simulated. The smeared image obtained due to poor quality PSF was improved by means of a Wiener Filter based deconvolution method. In this context the deconvolution method is rather simplistic and this issue will form the basis of further research. It will be interesting to explore other deconvolution techniques like blind de-convolution.

The results have demonstrated that this method can be used in high resolution terrain and change monitoring applications to obtain low cost and detailed images of a fixed location. However, it is understood that in a practical situation the resultant image might be severely degraded, the objective of further research efforts is to improve and bring the image as close to the ideal as possible. Some of the factors having an adverse effect on the signal include noise, strength of reflected signals, direct signal interference, atmospheric effects, radar clutter or backscatter and hardware limitations.

REFERENCES

A Komjathy, J. A. M., V U Zavorotny, P Axelrad and S J Katzberg (2000), ***Towards GPS Surface Reflection Remote Sensing of Sea Ice Conditions***, Sixth Int. Conf. on Remote Sensing for Marine & Coastal Environments.

Cardillo, G. P. (1990), "***On the use of Gradient to determine bistatic SAR resolution***", IEEE Antennas and Propagation Society International Symposium.

Cherniakov, M., He, X., , Zeng, T. (2005), "***Signal detectability in SS-BSAR with GNSS non-cooperative transmitter***", IEEE Proceedings-Radar Sonar and Navigation 152(3): 124-132.

Cherniakov, M., Zeng, T. and Plakidis, E. (2003), ***Ambiguity Function for Bistatic SAR and its Application in SS-BSAR Performance Analysis. Radar Conference***, Adelaide, Australia.

Cherniakov, M., Zeng, T., Long, T. (2005), "***Generalized approach to resolution analysis in BSAR***", IEEE Transactions on Aerospace and Electronic Systems 41(2): 461-474.

Cherniakov, M. N., D. Kubik, K. (2002), "***Air target detection via bistatic radar based on LEOS communication signals***", IEEE Proceedings-Radar Sonar and Navigation 149(1): 33-38.

D Masters, S. K., P Axelrad (2003), ***Airborne GPS Bistatic Radar Soil Moisture Measurements during SMEX02***, Proceedings of IEEE International IGARSS.

E. P. Glennon, A. G. D. "***A Review of GPS Cross Correlation Mitigation Techniques***", The 2004 International Symposium on GNSS/GPS, 2004.

Glennon, E., Dempster, AG and Rizos, CR (2006), "***Feasibility of air target detection using GPS as a bistatic radar***", Journal of Global Positioning Systems 5(1-2), pp. 119-126.

Griffiths, H. D. (2004), ***Bistatic and Multistatic Radar***, IEE Military Radar Seminar. Shrivenham, UK.

James L Garrison, A. K., Valery U Zavorotny, and Stephen J Katzberg (2002), "***Wind Speed Measurement using Forward Scattered GPS Signals***", IEEE Transactions on Geo-Science And Remote Sensing Vol. 40, (No. 1).

Kaplan, E. D. and C. Hegarty (2005), ***Understanding GPS Principles and application***, Artech House Publishers.

M Usman, D. W. A. (2008), ***Acquisition of Reflected GPS Signals for Remote Sensing Applications***, Proceedings of ICAST 2008, Islamabad.

M Usman, D. W. A. (2008), ***De-Convolution of images obtained by Correlation of Direct and Reflected GPS Signals***, 6th International Bhurban Conference on Applied Sciences and Technology. Islamabad, Pakistan.

M. Usman, D. W. A. (2006), ***A Remote Imaging System Based on Reflected GPS Signals***, ICAST 2006. Islamabad, Pakistan.

Martin-Neira, M. (1993), "***A Passive Reflectometry and Interferometry System (PARIS): Application to Ocean Altimetry***", ESA J vol. 17(331-335).

Peyton Z. Peebles, J. (2002), ***Radar Principles***, John Wiley & Sons, Inc.

R. C. Gonzalez, R. E. W. (2002), "***Digital Image Processing***", Prentice-Hall Inc.

Sklar, B. (2001), ***Digital Communication Fundamentals and Application***, Prentice Hall International Edition.

Smyth, T. (2008), ***Waveshaping Synthesis***, School of Computing Science, Simon Fraser University.

Soumekh, M. (1999), ***Synthetic Aperture Radar signal processing with Mat lab Algorithms***, John Wiley & Sons, Inc.

Stephen J. Katzberg and James L. Garrison, J. L. (1996), ***Utilizing GPS To Determine Ionospheric Delay Over the Ocean***, Virginia, USA, Research Center Hampton.

Yonghong Li, C. R., Eugene Donskoi, John Homer, Bijan Mojarrabi (2002), "***3D Multistatic SAR System for Terrain Imaging based on Indirect GPS Signals***", Journal of Global positioning system Vol. 1(No. 1): 34-39.

The corresponding author

Mohammad Usman (usman163@hotmail.com)**,** School of Electrical and Electronic Engineering, The University of Manchester, UK.